Geochemistry, Geophysics, Geosystems

RESEARCH ARTICLE
10.1029/2020GC009614

Special Section:
Magmatic and volcanic processes in continental rifts

Lower Crustal Earthquakes in the March 2018 Sequence Along the Western Margin of Afar

Alessandro La Rosa[1,2], Derek Keir[2,3], Cecile Doubre[4], Federico Sani[2], Giacomo Corti[5], Sylvie Leroy[6], Atalay Ayele[7], and Carolina Pagli[1]

[1]Dipartimento di Scienze della Terra, Università di Pisa, Pisa, Italy, [2]Dipartimento di Scienze della Terra, Università degli Studi di Firenze, Firenze, Italy, [3]School of Ocean and Earth Science, University of Southampton, Southampton, UK, [4]Institut Terre et Environnement de Strasbourg, University of Strasbourg/EOST/ENGEES, CNRS UMR 7063, Strasbourg Cedex, France, [5]CNR, Consiglio Nazionale delle Ricerche, Istituto di Geoscienze e Georisorse, U.O. Firenze, Firenze, Italy, [6]Institute des Sciences de la Terre de Paris, ISTeP, Sorbonne Université, CNRS, Paris, France, [7]Institute of Geophysics, Space Science and Astronomy, Addis Ababa University, Addis Ababa, Ethiopia

Abstract During the evolution of continental rift systems, extension is thought to progressively focus in-rift to the future breakup boundary while faults along the rift margins progressively deactivate. However, observational constraints on how strain is partitioned between rift axis and rift margins are still lacking. The Afar rift records the latest stages of rifting and incipient continental breakup. Here, we analyzed the recent M_W 5.2 earthquake on the Western Afar Margin on March 24, 2018 and the associated seismic sequence of >500 earthquakes using 24 temporary seismic stations deployed during 2017–2018. We show seismicity occurring at lower crustal depths, from ~15 to ~30 km, with focal mechanisms and relocated earthquakes highlighting both west-dipping and east-dipping normal faults. We tested earthquake depth using InSAR by processing six independent interferograms using Sentinel-1 data acquired from both ascending and descending tracks. None of them shows evidence of surface deformation. We tested possible ranges of depth by producing forward models for a fault located at progressively increasing depths. Models show that surface deformation is not significant for fault slip at depths greater than 15 km, in agreement with the hypocentral depth of 19 km derived from seismic data for the largest earthquake. Due to the localized nature of deep earthquakes near hot springs coupled with subsurface evidence for magmatism, we favor an interpretation of seismicity induced by migrating fluids such as magma or CO_2. We suggest that deep fluid migration can occur at the rifted-margin influencing seismicity during incipient continental rupture.

Plain Language Summary The Earth's continents are thinned and broken by extensional forces along rift valleys. Rift valleys are bounded by big fractures (called border faults) that form at the inception of extension and that slip causing earthquakes. As thinning proceeds, molten rock (magma) can rise making its way through the crust. It is not well understood where and how the molten rocks migrate through the crust, and whether, e.g., the large border faults are exploited as pathways. The migration of magma, and the gasses and fluids it releases, can fracture rock causing earthquakes. In this study, we analyzed earthquakes occurring along border faults of the Afar rift of Ethiopia. We found that they occur deep in the crust where previous studies indicate the presence of magma. Our results could suggest that border faults could keep slipping and causing earthquakes as a result of the migration of magma into the deep parts of the crust.

Key Points:
- We studied fault activity and kinematics at the Western Afar Margin using seismicity and InSAR
- We observed a seismic sequence occurring in the lower crust along both west-dipping and east-dipping faults
- Deep seismicity could be caused by fluid migration in the lower crust

Supporting Information:
Supporting Information may be found in the online version of this article.

Correspondence to:
A. La Rosa,
alessandro.larosa@unifi.it

Citation:
La Rosa, A., Keir, D., Doubre, C., Sani, F., Corti, G., Leroy, S., et al. (2021). Lower crustal earthquakes in the March 2018 sequence along the Western Margin of Afar. *Geochemistry, Geophysics, Geosystems*, *22*, e2020GC009614. https://doi.org/10.1029/2020GC009614

Received 22 DEC 2020
Accepted 6 MAR 2021

1. Introduction

During the early stages of continental rifting, extension generally focuses at the rift margin along large-offset border faults. As rifting proceeds, extension is thought to migrate to a narrow zone in the rift valley floor (Corti, 2009; Manighetti et al., 2001; Stab et al., 2016; Wolfenden et al., 2005). In magma-rich settings, the narrow zone of extension occurs in a series of ~70 km long, ~20 km wide *en-echelon* magmatic segments which host active volcanoes producing significant eruptions and intrusions (Hayward & Ebinger, 1996; Wright et al., 2012). The magmatic segments are interpreted to be the initiation of the future breakup plate boundary where seafloor spreading initiates (Keranen et al., 2004; Wright et al., 2006), while the border faults progressively deactivate and eventually become passive margins after seafloor spreading

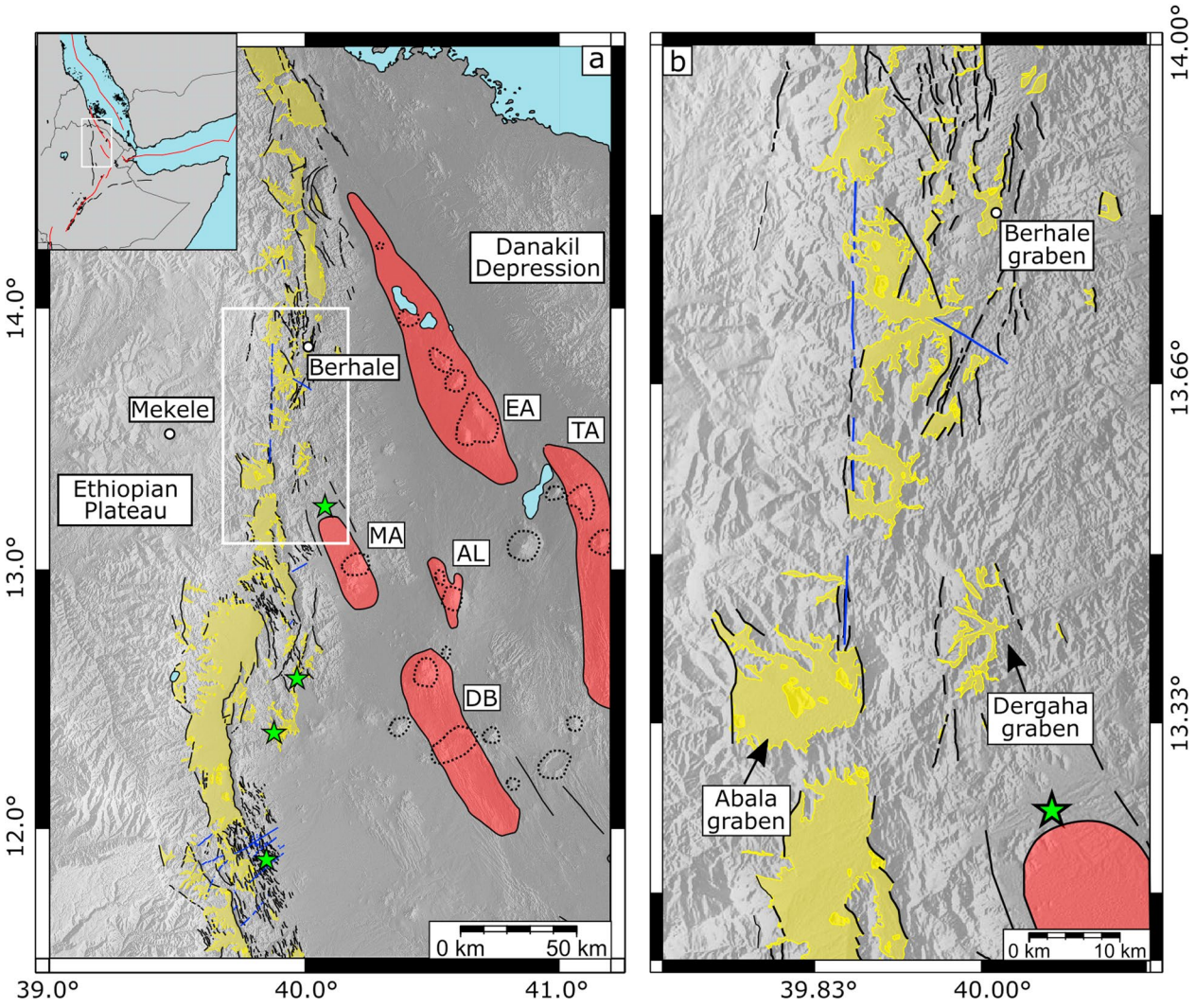

Figure 1. (a) Tectonic map of North-Western Afar showing the magmatic segments (red polygons) and associated volcanoes (black dashed lines), the marginal grabens (yellow polygons) along with major faults (black solid lines) and Miocene dikes (blue lines) identified in the area by Zwaan, Corti, Keir, et al. (2020), Zwaan et al., 2020b. The map also shows the hydrothermal springs (green stars) reported along the Western Afar Margin (WAM) by Keir et al. (2009) and the main active magmatic segments (red polygons) accommodating extension at the rift axis. EA, Erta Ale; TA, Tat Ali; AL, Alayta; DB, Dabbahu; MA, Ma'Alalta. (b) Close up on the study area showing the main marginal grabens and structures, as represented in (a).

starts (Hayward & Ebinger, 1996; Pagli et al., 2014). However, recent seismic observations at mature continental rifts show both intense fault-related seismicity (e.g., Ayele et al., 2007; Illsley-Kemp et al., 2018), and magmatic intrusion (e.g., Ebinger & Belachew, 2010; Pallister et al., 2010) characterizing the incipient passive margins of the Aden, Red Sea, and Afar rifts. This posed several questions regarding the dynamics of faulting, the causes of seismicity, and the related seismic hazard along mature rift margins.

The Afar rift is the locus of separation between the Nubian, Arabian, and Somalian Plates. A wide body of geological and geophysical observations (e.g., Barberi Tazieff, et al., 1972; Keir et al., 2013; Makris & Ginzburg, 1987) indicates that continental breakup is imminent in Afar. Large-scale systems of extensional faults (referred to as "Western Afar Margin"—WAM) bound Afar to the west separating the rift floor from the uplifted Ethiopian Plateau. Here, the interplay between synthetic (east-dipping) and antithetic (west-dipping) faults shape a series of seismically active marginal grabens which can be observed along the entire margin (Figure 1) (Chorowicz et al., 1999; Mohr & Gouin, 1976; Stab et al., 2016; Zwaan Corti, Keir, et al., 2020).

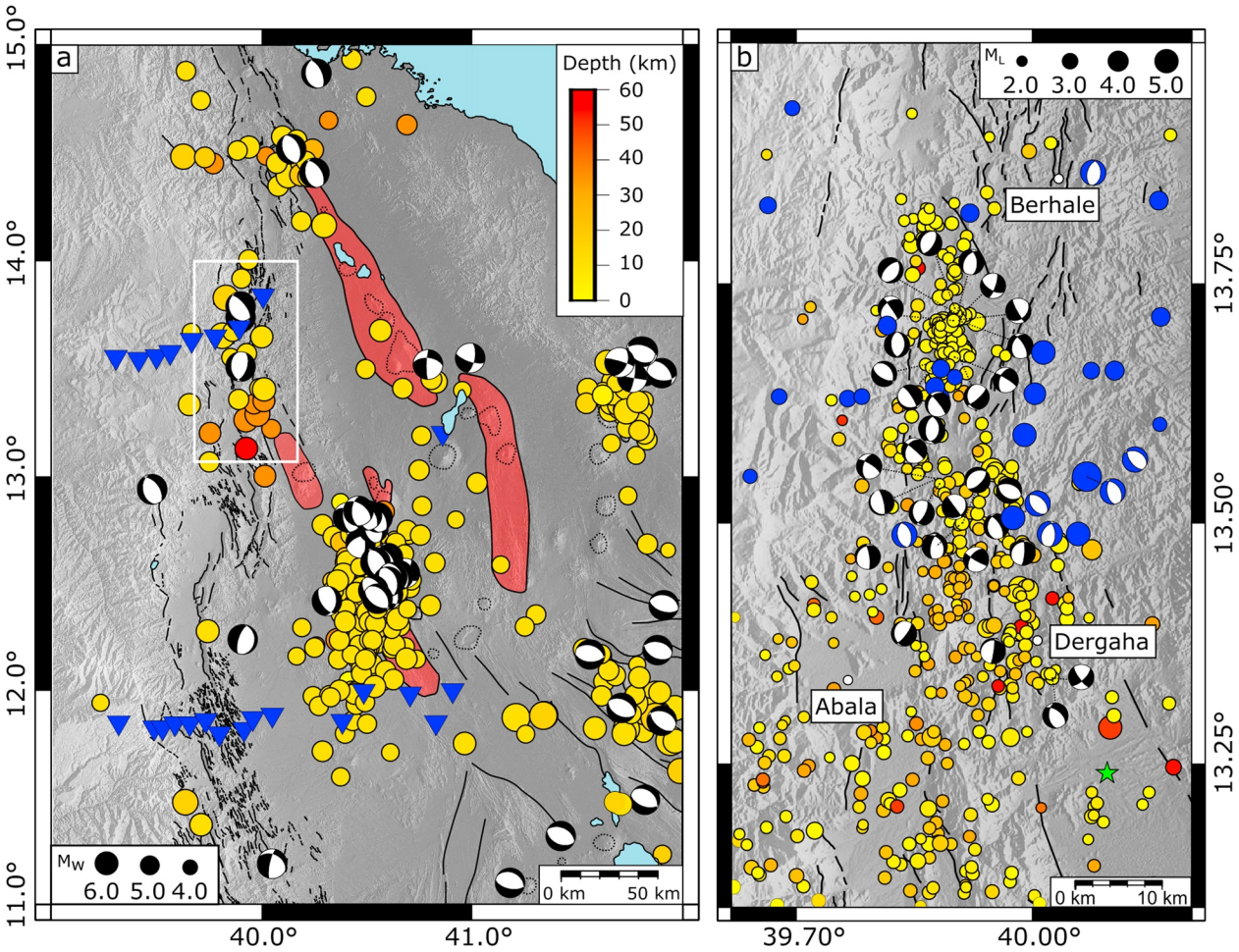

Figure 2. (a) Seismicity in Afar between 1973 and 2020 from the National Earthquake Information Centre (NEIC) and focal mechanisms from the Global Centroid Moment Tensor (GCMT) catalog. The blue reversed triangles are the seismic stations used in this study (Doubre et al., 2017; Keir et al., 2017). The white box marks the area shown in (b). (b) Local seismicity between 2005 and 2013 (Ayele et al., 2007; Zwaan et al., 2020a). The blue circles and focal mechanisms refer to the sequence of August 2002 (Ayele et al., 2007) (the depth informations are not available). Black focal mechanisms are from the 2011–2013 period (Illsley-Kemp et al., 2018; Zwaan et al., 2020b).

The Northern WAM (NWAM), east of the Tigray capital city of Mekele (at latitudes of N13°–N14°), displays the highest seismic activity along the entire WAM. Decades of recording from global seismic networks have shown the margin is seismically active with several $M_W > 5$ earthquakes occurring within the systems of marginal grabens (Figure 2, USGS National Earthquake Information Centre-NEIC). Intermittent temporary local seismic deployments show microseismicity in the upper crust (<15 km deep) is common (Figure 2) with lower crustal seismicity (15–30 km) being less common (Ayele et al., 2007; Belachew et al., 2011; Illsley-Kemp et al., 2018).

Recently, an M_W 5.2 earthquake struck the NWAM on March 24, 2018. Here, we analyzed the associated seismic sequence by using continuous recordings from the more recent temporary and high-density seismic network in Afar (Doubre et al., 2017; Keir et al., 2017) to investigate the fault activity and kinematics along the NWAM. Earthquakes were located at mid-to-low crustal depths (15–30 km) and the accuracy of hypocentral distribution has been evaluated through a series of simulated interferograms. A series of focal mechanisms were produced to analyze the kinematics of faulting during the seismic sequence. Our observations show that low crustal earthquakes occur at the NWAM during incipient continental breakup. In the same area, previous independent geophysical observations suggest the presence of melt emplaced in the lower crust (Hammond et al., 2011; Korostelev et al., 2015). Fluid migration from such emplaced melt is interpreted to influence seismicity and fault activity in the area.

2. Tectonic Setting

The Afar depression is bounded to the west by systems of tens of km long, ~NS-trending normal faults which define the margin from latitude N9.5° to N15° (Beyene & Abdelsalam, 2005). Steep, synthetic east-dipping fault scarps with ~1,000 m high throws mark the sharpest decrease in elevation from the plateau to the Danakil Depression (Beyene & Abdelsalam, 2005; Sembroni et al., 2017; Zwaan, Corti, Keir, et al., 2020). However, antithetic west-dipping normal faults dominate the architecture of several parts of the WAM producing eastward tilted blocks and a series of *en-echelon* right-stepping marginal grabens (Baker et al., 1972; Beyene & Abdelsalam, 2005; Stab et al., 2016; Zwaan, Corti, Keir, et al., 2020). The tilted blocks are evident south of N12.5° showing a dip angle increasing rift-ward from 10° to 45° and are controlled by west-dipping faults with dip angles up to 70° Zwaan, Corti, Keir, et al., 2020; Zwaan et al., 2020a. The marginal grabens are generally 10–30 km long, strike in an NNW-SSE direction, oblique with respect to the general NS orientation of the WAM (Figure 1), and are connected by complex transfer zones which result in a right-stepping geometry (Beyene & Abdelsalam, 2005; Chorowicz et al., 1999; Zwaan, Corti, Keir, et al., 2020; Zwaan et al., 2020a). Dense drainage networks crosscut the WAM from west to east eroding the faulted blocks and depositing sediments within the adjacent basins. Geochronological data suggest that fault activity at the WAM began in the Oligocene (Ayalew et al., 2006; Wolfenden et al., 2005), but the inception of marginal grabens formation at the WAM is still debated. Dating of alluvial deposits filling some of the marginal grabens in the northern sector of the WAM suggests that they started forming during the Pliocene (e.g., Beyene & Abdelsalam, 2005; Chorowicz et al., 1999). However, in most cases, dating at the base of alluvial deposits is not available and the age of marginal grabens is poorly constrained (e.g., Tesfaye & Ghebreab, 2013).

On the Plateau, east of the Mekele city, between N12.5° and N14.0°, a 2,000 m elevated region of Mesozoic marine sediment outcrops and overlays the Precambrian metamorphic basement. The entire sequence is intruded by Miocene dykes (Figure 1) and sills (Sembroni et al., 2017; Zwaan et al., 2020a). Systems of east-dipping and west-dipping normal faults form a series of marginal grabens of which some are the Berhale, Abala (Zwaan, Corti, Keir, et al., 2020), and Dergaha grabens (Gouin, 1979) (Figure 1b). The marginal grabens have the same NNE-SSW trend observed elsewhere along the WAM, south of N12°. However, unlike other sectors of the WAM where the marginal grabens are well developed and have sharp margins and clear fault surfaces, smaller and less developed basins have been observed between N13° and N14° (e.g., Dergaha, Figure 1) (Zwaan, Corti, Keir, et al., 2020; Zwaan et al., 2020a). Structural field measurements in the Abala graben report an extension direction of ~N80°E (Zwaan et al., 2020a) while in the other adjacent grabens no measurements have been made. Finally, hydrothermal activity with hot springs is also reported 20 km south of Dergaha (Figure 1) (Keir et al., 2009).

The decrease in topographic elevation caused by the activity of the border fault systems at the WAM is mirrored by a progressive crustal thinning toward the rift valley. Several seismic studies (Hammond et al., 2011; Maguire et al., 2006; Makris & Ginzburg, 1987) showed that the variation in topographic elevations across the WAM is accompanied by strong variations in crustal thickness and Vp/Vs ratios. In Northern Afar, the crust thins eastward from ~38 km below the Ethiopian plateau to ~16 km beneath the Danakil Depression, with most of the thinning occurring across the WAM. Progressive crustal thinning and decreasing elevation toward the rift axis also characterize the rift floor which reaches minimum elevations between 50 and 100 m below sea level at the Danakil Depression (Hammond et al., 2011). South of ~N11°, the crust below the plateau is thicker (~40 km) and thins eastward to ~20 km into the rift. Low Vp/Vs ratios (1.7–1.8) characterize the thick felsic crust at the plateau, yet anomalously high Vp/Vs values (1.9–2.0) have been measured beneath the Dergaha graben (Hammond et al., 2011). Similar values characterize the mafic crust of the rift valley. Additionally, Korostelev et al. (2015) and Chambers et al. (2019) used ambient noise tomography and imaged a pattern of slow seismic wave speeds focused right beneath our study area, between the lower crust and upper mantle. Both high Vp/Vs and slow seismic velocities have been interpreted as related to the presence of melt and fluids (Chambers et al., 2019; Hammond et al., 2011; Korostelev et al., 2015).

2.1. Seismicity at North-Western Afar Margin (NWAM)

Figure 2 shows the seismicity recorded by both global (Figure 2a) and local (temporary) (Figure 2b) networks in the study area. Seismic activity in the NWAM is characterized by several $M_W > 5.0$ earthquakes

that occurred during the last few decades. In general, seismicity located by both local and global catalogs at the margin is located in the upper crust (<15 km), with deeper seismicity focused in the lower crust (>15 km) being much less common (Illsley-Kemp et al., 2018; USGS NEIC catalog). The first seismic sequence instrumentally recorded in the area is that of April 1989 (USGS NEIC catalog). The episode includes two earthquakes with $M_W > 5.0$ and several $M_W > 4.0$ earthquakes at the southern tip of the Dergaha and Abala grabens, between N13.2° and N13.4° (Figure 2a). Relatively deep hypocenters, between 10 and 33 km, are reported in global catalogs for these episodes, though due to the large error bars in the NEIC catalog the depths are in reality poorly constrained (Figure 2a). Further north, between N13.5° and N13.8°, a sequence of 75 aftershocks ($M_W \leq 5.0$) accompanied a main shock with M_W 5.6 in August 2002 (Ayele et al., 2007). Moment tensor inversion of locally recorded waveforms provided focal mechanisms for six of these events, all consistent with normal faulting along NNW-striking and NE-dipping planes (Figure 2b) (Ayele et al., 2007). The source depth of the main events deduced from moment tensor inversion of local broadband waveform data is estimated at 5–7 km (Ayele et al., 2007). Recomputation of moment tensors of the larger earthquakes along the WAM from regional and global waveforms also yields similarly shallow depths (<10 km) (Craig et al., 2011).

More recently, the temporary seismic networks implemented between 2005–2009 (Belachew et al., 2011; Ebinger et al., 2008) and 2011–2013 (Illsley-Kemp et al., 2018) recorded >1,900 low-magnitude earthquakes ($0.3 < M_L > 4.5$) north of the Dergaha graben (Figure 2b) suggesting that seismicity along the NWAM is persistent. Furthermore, several indications, such as the *b*-value, the double-couple mechanisms, and the high-frequencies of the earthquake waveforms were interpreted to indicate that the origin of this seismicity is mainly tectonic (Illsley-Kemp et al., 2018). The hypocentral distribution during the 2011–2013 period highlights ~NS-striking, west-dipping faults with seismicity mainly clustered at depths <15 km but with some located deeper than 20 km near to the Abala graben (Illsley-Kemp et al., 2018; Zwaan, Corti, Keir, et al., 2020). The focal solutions indicate oblique faulting characterized by both normal and strike-slip component and (Figure 2b) accommodating a N82°E-trending extension, suggesting that extension along the NWAM occurs mainly along west-dipping normal faults. Similar structural architecture has also been observed in other parts of the WAM, south of latitude N12° (e.g., Stab et al., 2016).

3. Earthquake Location and Magnitude Estimation

Twenty-four stations from two recent temporary seismic networks installed in Afar (Figure 2a) (Doubre et al., 2017; Keir et al., 2017) were operational on March 24, 2018 when the M_W 5.2 earthquake struck the NWAM, east of Mekele. We visually inspected 41 days of continuous seismic recordings, from March 20 to April 30, 2018 and manually picked both *P* and *S* waves for earthquakes recorded by four or more stations (Text S1). We located the events using the Oct-Tree search algorithm implemented into the NLLoc software (Lomax et al., 2000).

For the location, we used a 2.5D seismic velocity model reproducing the large-scale crustal structure of the WAM (Text S2). A correct velocity model and an accurate Vp/Vs ratio are crucial for a precise earthquake location. However, this is challenging to obtain, especially for complex crustal structures and variable Vp/Vs values as it has been observed at the WAM by Makris and Ginzburg (1987), Maguire et al. (2006), and Hammond et al. (2011). Starting from these observations, we created a 2D velocity profile cross-cutting both the Afar margin and axis in an EW direction, along a distance of 250 km (Text S2 and Figure S1a). The profile has been then extended to 250 km along the third dimension (NS in this case) to create a 2.5D grid. We made a model characterized by crustal features intermediate between the Northern and the Central Afar, where the seismic stations and the study areas are located (Figures 2a and S1a). The velocity model has a crustal thickness of 35 km below the Ethiopian plateau which gradually decreases to 18 km at the rift axis (Text S2 and Figure S1a). The topography has also been reproduced with elevations varying from 2 km at the plateau to 0.5 km at the axis. The crustal structure is made of four layers encompassing the cover rocks, the basalts, the upper crust, and the lower crust, with velocities gradually increasing from 4.4 km/s of the cover rocks to 6.8 km/s at the base of the lower crust. An additional shallow low velocity layer (3.3 km/s) was introduced in the rift zone to reproduce the recent sediments. Finally, an upper mantle with uniform velocity of 7.4 km/s completes the model (Text S2 and Figure S1a).

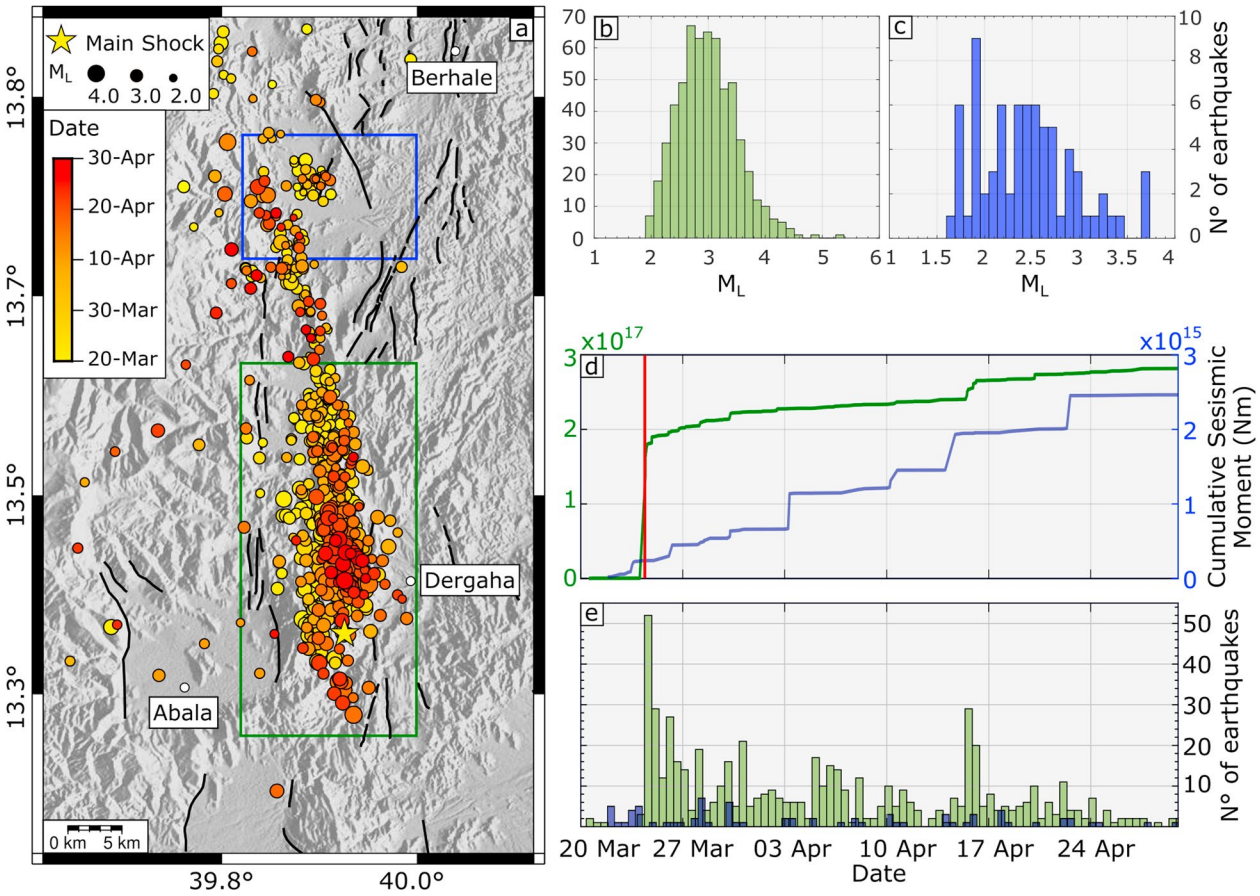

Figure 3. (a) Epicentral distribution of the 673 earthquakes located with NLLoc (Lomax, 2000) and occurred between March 20, 2018 and April 30, 2018. The earthquakes are color-coded by time. The blue and green boxes highlight the two marginal grabens along the North-Western Afar Margin (NWAM). (b and c) Histograms of magnitudes for the two areas highlighted in (a). (d and e) Cumulative seismic moment curves and histograms of number of earthquakes for the two areas in (a).

Since high variability in Vp/Vs characterizes the margins where our network was located, we tested several Vp/Vs and produced Wadati diagrams in order to find a value corresponding to an average through the model (Figure S1b). We found minimum residuals for Vp/Vs of 1.74 which average those measured by Hammond et al. (2011) at the stations along WAM (Figure S1b). However, our Wadati diagram does show that the stations within the rift on the southern profile show a distinctively higher Vp/Vs of 1.85, but these contribute only ~36% of total arrivals.

The local magnitude (M_L) for each earthquake has been calculated by measuring the zero-to-peak amplitude on simulated Wood Anderson seismometers, and using the distance correction for the Danakil Depression from Illsley-Kemp et al. (2017).

We located 673 events on the NWAM (Figure 3a and Table S1) with average vertical and horizontal errors of ±4.8 and ±6.6 km, respectively. Hypocentral depths and related uncertainties are reported in Figure S2, where we report just earthquakes with both horizontal and vertical errors lower than 6 km. Further details on the error calculation are also provided in the supporting information. The seismic catalog encompasses events with $M_L \geq 1.6$ with a mean magnitude uncertainty estimated as ±0.3 (Figures 3b and 3c). The local magnitude of the largest earthquake has been calculated as M_L 5.3 ± 0.4, close to the value of M_W 5.2 reported by the NEIC. The largest earthquake occurred at a depth of ~19 ± 4 km, where most of the hypocenters also focused. We identified two areas of clustered seismicity characterized by distinct spatial and temporal distributions (Figure 3). The main seismic sequence of March–April 2018 occurred within the Dergaha graben with 514 earthquakes located along a system of ~NS-striking faults bounding the graben to the west

(green box in Figure 3a). Hypocentral depths range between ~1 and ~30 km indicating that seismicity in this part of NWAM occurs throughout the entire crust.

Most of the seismic sequence (309 of the 514 events) occurred between March 24, 2018 (day of the main event) and March 31, 2018 with an average of 39 earthquakes per day. The seismicity rate progressively decays to a minimum of ~3 earthquakes per day by the April 30, 2018, comparable to the number of earthquakes that occurred in the days before the onset the seismic sequence (Figures 3d and 3e). However, another burst of activity is also observed on April 16, 2018, with the occurrence of 30 located earthquakes (Figures 3d and 3e).

Minor seismic activity is also observed within a small graben, south-west of Berhale, during the analyzed time period (blue box in Figure 3a). Seismicity is shallow, between 5 and 15 km (Figure S2) with 75 earthquakes scattered in time rather than clustered in seismic sequences, as observed in the Dergaha graben. Furthermore, the occurrence of the earthquakes in this area seems to be temporally independent from the main seismic sequence (Figures 3d and 3e). Interestingly, a pattern in the spatiotemporal distribution of earthquakes with low error in the hypocentral location can be inferred from the profiles in Figure S2. The main sequence takes place close to the southern tip of Dergaha at depth of 19–25 km, where the largest earthquake occurred. After that, earthquakes show a progression to shallower crustal levels and toward the northern tip of Dergaha which could indicate a migration of seismicity.

To improve the resolution of hypocenter locations and highlight active fault planes, we relocated 262 earthquakes using the double-difference method implemented in the HypoDD software and a minimum of 10 observations per event pair (Waldhauser, 2001; Waldhauser & Ellsworth, 2000). The relocated seismicity highlights both east-dipping and west-dipping active fault planes bounding the western side of the Dergaha graben (Figures 4a and 4b). We interpret the sharp alignments of seismicity as illuminating the fault planes between 15 and 30 km (Figure 4b). In addition, the projection of the west-dipping plane to the surface clearly matches the topographic expression of a fault represented by a scarp separating the Dergaha graben from the adjacent horst (Figure 4b). The distribution of seismicity also shows a main fault plane dipping to the west while a conjugate east-dipping fault is just observed at the northern tip of the Dergaha graben.

4. Focal Mechanisms

We computed focal mechanisms based on the polarities of the *P* wave arrivals at both northern and southern stations. *P* wave arrival polarities of events recorded by >15 stations have been processed using FOCMEC software (Snoke, 2003). Focal solutions have been attempted only for earthquakes with unambiguous first arrivals and no polarity errors have been allowed. This resulted in well resolved focal mechanisms with maximum standard deviations (σ) in strike and dip angles of the possible solutions equal to 7.5° and 11°, respectively (Table 1). We considered the nodal planes subparallel to the faults reported in literature (i.e., ~NS) as the main ones and classified their kinematics on the basis of the rake value. *P* and *T* axes of each solution have been used to retrieve the average extensional direction along the NWAM.

Twenty well-constrained focal mechanisms were obtained for earthquakes within the Dergaha graben. All the solutions have main nodal planes oriented ~NS (Figure 4 and Table 1). The focal solutions are characterized by dominant normal faulting along ~NS-striking faults, associated with a minor lateral component (Figures 4a and 4b). Ten focal mechanisms related to the major events can be observed along the central and southern part of the Dergaha graben and show normal faulting with minor oblique right-lateral slip on steep (57°–84°), west-dipping planes (Figures 4a and 4c, Table 1). Conversely, normal faulting earthquakes with minor oblique left-lateral slip along east-dipping planes mainly focus along the northern tip of the Dergaha graben (Figures 4a and 4c, Table 1). Three pure dip-slip focal mechanisms are also present in the central part of the graben, with both east-dipping and west-dipping planes (Figures 4a and 4c, Table 1). *P* and *T* axes computed from all the solutions indicate an average N092°E-trending extension, nearly orthogonal to the average strike of the faults observed in this area of the NWAM. The main nodal planes match very well with the structures observed in the field by Zwaan et al. (2020a) as well as the fault planes deduced from the relocated seismicity (Figure 4).

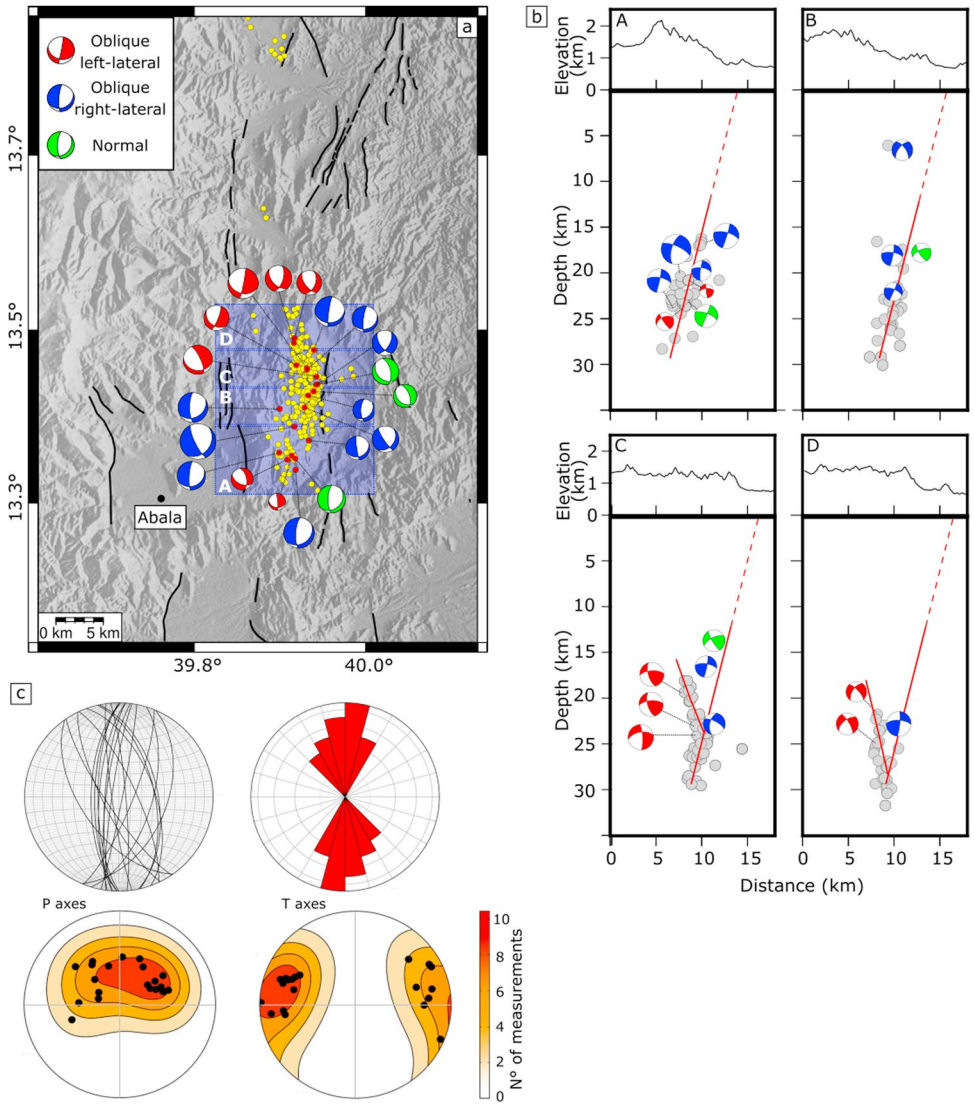

Figure 4. Focal mechanism solutions in map view (a) and cross sections (b) for events located with >15 stations. Yellow dots in (a) and gray dots in (b) are the relocated seismicity. Red lines in (b) represents possible faults highlighted by the relocated seismicity. (c) The plots show the stereographic projection of the strike and dip (top left), the rose diagram of the strikes (top right), and the *P* and *T* axes of the main nodal planes with contour of number of measurements (bottom).

5. Interferometric Synthetic Aperture Radar (InSAR)

InSAR is widely used to identify coseismic surface displacements and investigate the earthquake source parameters. However, the ability of InSAR to detect coseismic surface deformation strongly depends on the noise level affecting the interferometric phase (e.g., spatial and temporal decorrelations or atmospheric noise) along with the earthquake magnitude and the depth of the source (e.g., Dawson & Tregoning, 2007; Funning & Garcia, 2019).

In order to investigate the surface deformation related to the M_L 5.3 event of March 24, 2018, we processed six independent interferograms from C-band SAR images acquired by the Sentinel-1 satellite on both ascending (014) and descending (079) tracks (Figures 5a, 5b and S2). Six independent coseismic interferograms with temporal baselines ranging from 36 to 144 days were processed using the InSAR Scientific Computing Environment (ISCE) software developed by the Jet Propulsion Laboratory, Caltech and Stanford University (Rosen et al., 2012). The interferograms were coregistered and corrected from topography-correlated noise

Table 1
Parameters of the Focal Solutions Computed for 20 Major Earthquakes Occurred at Dergaha and Showed in 4

Date and UTC time	M_L	Strike	σ strike	Dip	σ dip	Rake	σ rake
March 24, 2018 10:27	5.3	154	3.9	76	6.9	−117	0.9
March 24, 2018 10:56	4.3	184	0.8	78	0	−113	0
March 24, 2018 11:23	4.0	146	0	79	0	−122	0
March 24, 2018 21:02	4.5	180	3.2	72	1.0	−117	3.1
March 25, 2018 01:48	3.3	348	3.6	56	4.0	−53	2.0
March 26, 2018 00:25	2.5	355	1.5	84	0.8	−61	0.5
March 26, 2018 00:29	4.2	181	4.6	69	7.6	−109	2.2
March 29, 2018 18:37	3.8	145	4.9	57	4.4	−141	6.2
March 30, 2018 06:31	4.6	184	1.3	73	3.3	−111	0.4
March 31, 2018 00:56	3.5	340	2.8	59	3.9	−74.5	0.9
April 02, 2018 11:02	3.8	22	1.7	78	4.0	−55	0.6
April 02, 2018 11:50	4.0	17	7.0	61	11.0	−50	9.0
April 07, 2018 19:49	3.9	187	2.3	79	3.4	−111	2.4
April 11, 2018 20:59	3.6	172	1.7	84	1.7	−116	0.4
April 15, 2018 12:11	4.6	11	0.8	87	1.7	−56	1.4
April 15, 2018 12:34	4.4	335	1.4	75	1.4	−68	0.7
April 15, 2018 13:23	4.0	347	4.7	59	6.4	−71	2.0
April 15, 2018 22:37	4.5	188	0.7	84	0	−114	0
April 20, 2018 03:34	3.7	23	7.5	48.5	7.8	−41	5.8
April 23, 2018 01:25	3.4	181	1.8	66.5	3.1	−114	0.7

Note. Sigma (σ) is the standard deviation calculated from the range of solutions provided by FOCMEC for each main nodal plane.

using a standard 1 arc-sec SRTM Digital Elevation Model (DEM) (Farr et al., 2007). We then applied a standard power spectrum filter (Goldstein & Werner, 1998) of 0.5 and unwrapped the interferograms using the branch cut method (Goldstein et al., 1988). The interferograms were finally geocoded at a final pixel spacing of 30 m using the 1 arc-sec DEM. The Sentinel-1 interferograms have relatively low level of noise and maintain good coherence up to temporal baseline of 144 days (Figure S3). However, no significant deformation has been identified in any of the coseismic interferograms in the epicentral area (Figures 5a, 5b and S2) suggesting that coseismic slip occurred at large depth and caused too small surface deformation to be measured by InSAR, as also indicated by the deep source location obtained from seismic data. To test this hypothesis, we produced a series of simulated interferograms assuming different depth of possible fault slip. We used an Okada shear dislocation within a homogeneous, elastic half-space with a Poisson's ratio of 0.25 and a shear modulus (μ) of 3.2×10^{10} Pa (Okada, 1985). We assumed a 10 km × 10 km normal fault, striking NS and dipping to the west with an angle of 70°, following the hypocenter distribution and the fault geometry deduced from the focal mechanisms (Figure 4 and Table 1). Normal slip was fixed at 245 mm to simulate an M_W 5.2, as reported by the USGS NEIC catalog. We produced forward models using the incidence angles from descending tracks 079 to estimate the surface displacement field in the Line-of-Sight (LOS) component of the InSAR measurements assuming a progressively increasing depth of the fault top edge between 1 and 15 km, with a step size of 5 km (Figures 5c–5f). The simulations show that LOS displacement decreases rapidly at increasing depth of faulting. For a fault having the top edge at 15 km depth (and bottom edge at ~24 km depth) we see <1 cm of LOS displacement, which would be difficult to resolve in a single interferogram. Such a model is likely applicable to our observations of an earthquake with a hypocentral depth of ~19 km, and would cause a too small surface displacement to be detected by InSAR.

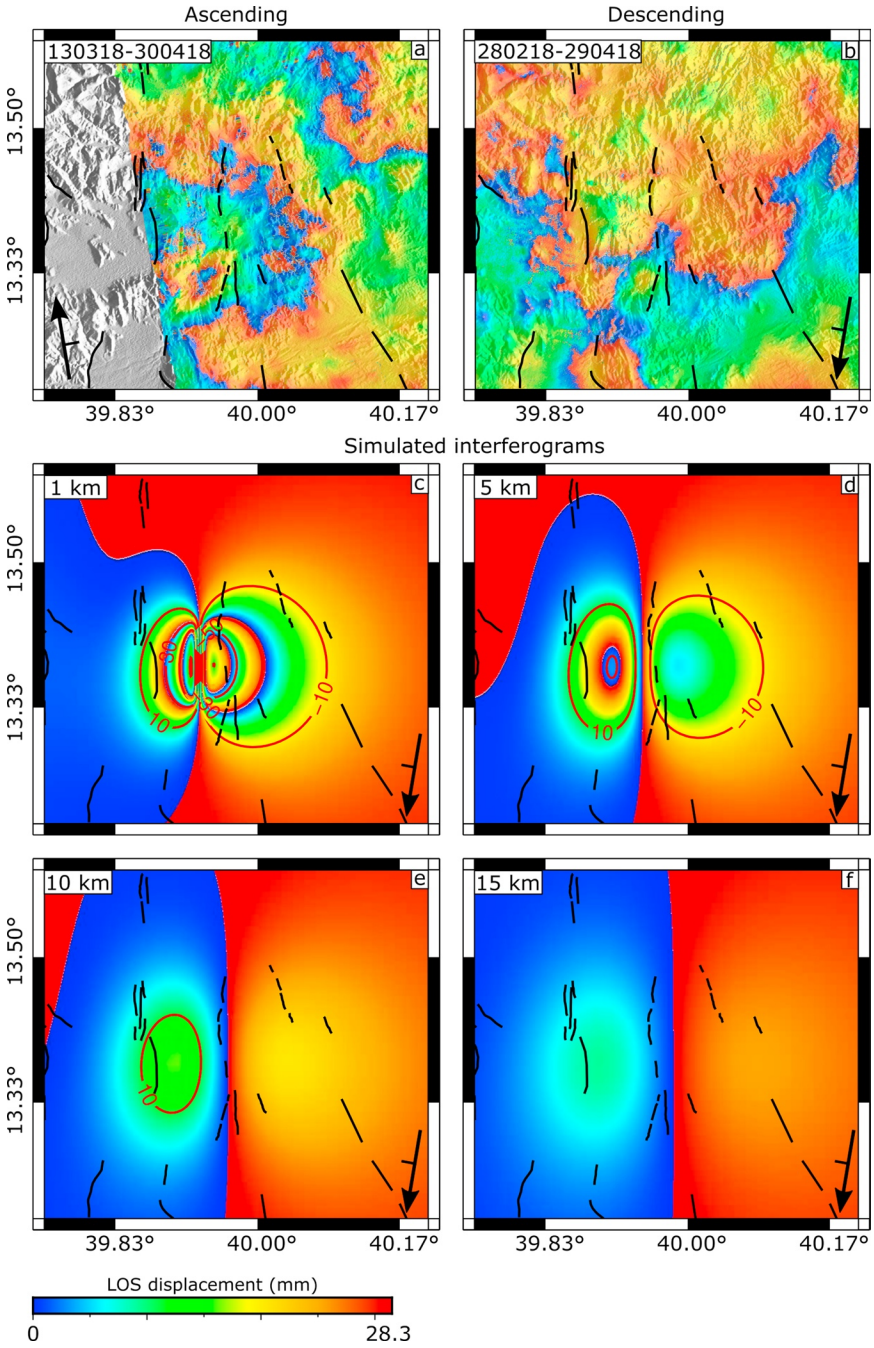

Figure 5. (a and b) Measured wrapped coseismic interferograms from Sentinel-1 acquisitions. (c–f) Simulated wrapped interferograms assuming Okada shear dislocation model located at increasing depth. The red contour lines display the unwrapped deformation in mm. Black solid lines are faults reported by Zwaan et al. (2020b).

6. Discussion

We analyzed the seismicity in a time period of 41 days, covering the M_L 5.3 of March 2018, to investigate the fault activity across the NWAM. Seismic location and well-constrained focal mechanisms give constraints on the fault kinematics characterizing the marginal grabens during the time period under study.

We observed earthquakes focused in an area of the NWAM (N13.3°–N13.8°) characterized by continuous seismicity and several $M_W > 5$ in the past few decades (Figure 2) (USGS, Ayele et al., 2007; Belachew

et al., 2011; Illsley-Kemp et al., 2018). The largest part of the catalog consists of the seismicity that occurred in the Dergaha graben and within the minor grabens to the north between March 24, 2018 and April 30, 2018. The results show the main seismic sequence was distributed through the entire crust, with the largest, M_L5.3, earthquake occurring at ~19 km and the other major earthquakes also located in the lower crust between 15 and 30 km (Figures 4b and S1b). InSAR data do not show any significant surface deformation related to the M_L 5.3, earthquake suggesting that the hypocentral depth of the episode was greater than 15 km (Figure 5), in agreement with the seismic results. Lower crustal depths in this region have already been reported in global catalogs for other $M_W > 5$ earthquakes in 1989–1990, as well as in local catalogs (Belachew et al., 2011; Illsley-Kemp et al., 2018; Zwaan et al., 2020a), suggesting that part of the seismic moment in this sector of the NWAM is released at greater depth. Conversely, the M_W 5.6 sequence of August 2002 close to Dergaha was shallower (5–15 km), as also the low-magnitude seismicity north of ~N°13.6 reported by Illsley-Kemp et al (2018) and Zwaan et al. (2020a) during the time period 2011–2013.

The relocated seismicity in the Dergaha graben clearly highlights two steep crustal faults with a main west-dipping fault and a conjugate east-dipping fault (Figure 4b). The latter seems to rupture just at the northern tip of the Dergaha graben. The fault planes deduced from the alignment of the seismic cluster are consistent with the orientation of nodal planes of the focal mechanisms. Together, the earthquake locations and the focal mechanisms indicate dominant normal faulting accompanied by a minor right-lateral slip along west-dipping faults at the southern and central parts of the Dergaha graben. To the north, the dominant normal component is instead associated with minor left-lateral slip along east-dipping faults. The structural setting of the two fault planes at Dergaha, along with the higher magnitude content of earthquakes occurring along west-dipping faults suggest that west-dipping faulting is dominant. The *T* axes calculated from the focal solutions indicate that the average extension direction is oriented ~EW. Structural field measurements in the Abala graben, along with the seismicity distribution and the focal mechanisms south of Berhale indicate similar extension directions and fault architecture (Zwaan et al., 2020a). About 130 shallow earthquakes along east-dipping and west-dipping faults in Dergaha have also been reported by Zwaan, Corti, Keir, et al. (2020; Zwaan et al., 2020a).

On the basis of the diffuse seismicity and the structural evidences of active faulting at surface, Zwaan et al. (2020a) suggested that extension is still ongoing along the NWAM. The spatial correspondence between our observations of dominant normal faulting and their structural and seismic data set are consistent. Additionally, we also show that deep seismicity occurs in this region and that dissimilarities between the temporal and spatial distributions of the seismicity in Dergaha and in the other sectors of the NWAM exist. In particular, the seismicity south of Berhale is spread over time and seems to occur independently from the main seismic sequence striking the Dergaha graben. Furthermore, our new observations of the 2018 sequence coupled with the ~50 years long NEIC catalog (Figure 2) showing deep earthquakes focused below the Dergaha graben suggests that the mechanism driving seismicity here may be different from that causing seismicity along the rest of the NWAM, where only upper crustal earthquakes are observed (e.g., Ayele et al., 2007; Illsley-Kemp et al., 2018; Zwaan et al., 2020a).

Deep earthquakes have been widely observed elsewhere at both mature and young basins along the East African Rift System (e.g., Main Ethiopian Rift, Keir et al., 2009; Lapins et al., 2020; Muluneh et al., 2020; Western Rift Branch, Albaric et al., 2009, 2014; Tanganyika Rift, Lavayssière et al., 2019; Shudofsky, 1985; Magadi-Natron basin, Lee et al., 2016) as well as other active rifts worldwide (e.g., Déverchère et al., 2001; Doser & Yarwood, 1994). Deep (15–30 km) moderate earthquakes ($M_W < 6.0$) occur across hundreds of kilometers-long segments of the Western and Eastern Rift Systems in Tanzania. Several authors (e.g., Albaric et al., 2009, 2014; Muluneh et al., 2020; Shudofsky, 1985) related such seismicity to the presence of a strong, intruded, mafic lower crust which can deform in a brittle manner at greater depths. The same mechanism has also been invoked by Déverchère et al. (2001) to explain deep seismicity in the Baikal rift. Similarly, Lavayssière et al. (2019) analyzed seismicity in the Rukwa and Tanganyika during 2014–2015 and suggest that deep earthquakes are related to the activity of steep border faults cross-cutting the entire crust, which is enabled by a cold lower crust and a very thick mantle lithosphere in the region (Craig et al., 2011). In contrast, Seno and Saito (1994) explained deep earthquakes across the East African Rift System as induced by the locally high strain rates induced by migration of fluids, such as from the upper mantle. Similarly, Lee et al. (2016) compared flux measurements and isotope compositions of CO_2 emissions with lower crustal

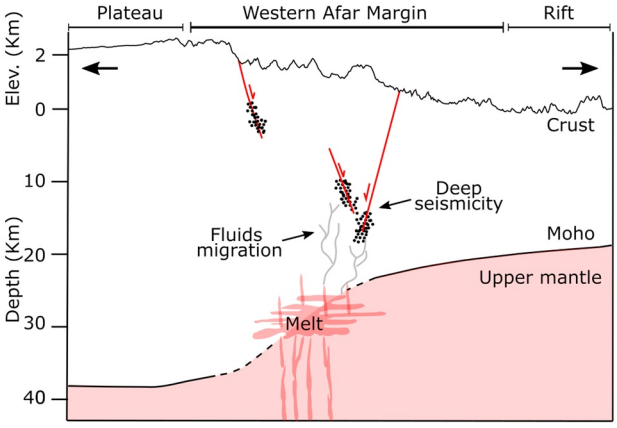

Figure 6. Simplified sketch showing the interpretation and proposed mechanism controlling the deep seismicity below the Dergaha graben. We interpret deep seismic activity along rift border faults to be induced by magma migration or the release of fluids such as mantle-derived CO_2.

earthquakes along large-offset fault scarps in the Magadi-Natron Basin (Kenya-Tanzania border) to suggest that deep seismicity (15–27 km) in the area is caused by tectonic degassing of mantle-derived CO_2. Deep seismicity has also been reported by Keir et al. (2009) near the flank of the Main Ethiopian Rift, where spatial associations between lower crustal earthquakes and high conductivities imaged in magneto-telluric data led them to propose that such seismicity is related to either melt migration or fluid circulation resultant from magma emplacement.

The presence of NS-oriented mafic dikes along the NWAM such as those observed between Berhale and Abala (Zwaan et al., 2020a) indicates that mafic intrusions have been emplaced below the NWAM in the past. Most of Miocene dykes are coeval with those observed along the margin of the Red Sea and likely associated with early magma-assisted rifting (e.g., Buck, 2006). A possible explanation for deep seismicity in the study area could thus be that the lower crust beneath the NWAM is mafic and therefore strong enough to be capable of brittle deformation at large depths. However, such a factor would likely facilitate deep seismicity along most of the WAM, like the large (several hundreds of km) along rift spatial extent of deep seismicity occurring in Tanzania and along the Baikal rifts (Albaric et al., 2009; Déverchère et al., 2001). Since we observe more localized deep seismicity, we therefore do not favor this explanation.

By comparing our results with other local and global seismic catalogs (e.g., Figure 2), we observe that the area showing deep seismicity in the NWAM is strongly focused around the Dergaha graben only. This brings us to hypothesize that a more local factor could play a role in triggering the deep earthquakes. Seismic imaging of the lithosphere by Hammond et al. (2011), Korostelev et al. (2015), and Chambers et al. (2019) have shown anomalously high Vp/Vs (~2.0) and slow seismic velocities beneath Dergaha which have been interpreted as due to the current presence of partial melt in the lower crust and upper mantle. The presence of magma is also supported by geological evidences of recent (0.12 ± 0.05 Ma) axial volcanism at the adjacent Ma'Alalta magmatic segment (Figure 1) (Barberi, Borsi, et al., 1972; Tortelli et al., 2020), which is heavily offset to the west to be close to the WAM. We thus hypothesize that the deep, focused seismicity in Dergaha could be induced by migration of either melt, or other fluids through the lower crust (Figure 6). Our interpretation of fluid induced seismicity here is also supported by the migration pattern of earthquakes toward shallow crustal levels and toward the northern tip of Dergaha (Figure S2), and the presence of microseismicity preceding the main sequence (Figure 3e) (Belachew et al., 2011; Illsley-Kemp et al., 2018, and this study). Patterns of earthquakes migration have been widely observed during seismic sequences, and in some case, they have been interpreted as induced by fluids (e.g., Antonioli et al., 2005; Yamada et al., 2015; Yoshida & Hasegawa, 2018). In addition, hot springs are present near the Dergaha graben, but absent further north where the earthquakes are only in the upper crust (Figure 1). The shape of the clusters together with their focal mechanisms would suggest that the fluids induce failure of deep fault systems connected to the upper crustal faults, as also suggested by the presence of hydrothermal activity in the area. Fluid induced fault slip could assist extension in the region by reducing the yield strength of the surrounding crust and triggering seismic slip along crustal faults as observed in the Main Ethiopian Rift (Keir et al., 2009; Lapins et al., 2020), in the Magadi-Natron Basin (Tanzania-Kenya) (Lee et al., 2016), in the Asal Rift (Djibouti) (Doubre & Peltzer, 2007), and along the magmatic rifted margin of the Red Sea (Blanchette et al., 2018). Deep seismicity in the Magadi-Natron Basin generated by tectonic degassing of mantle-derived CO_2 highlights the deep section of steep rift-parallel border faults (Lee et al., 2016), similar to what we observed in the Dergaha graben.

7. Conclusion

In this study, we provided new observations of the fault activity across the NWAM. We located 673 during the time period between March 20, 2018 and April 30, 2018, covering the seismic sequence of March 2018, east of Mekele. The sequence started on March 24, 2018 with an M_L 5.3 earthquake rupturing the deep

portion (15–30 km) of tens of kilometers-long crustal faults in the Dergaha graben, where other deep seismic sequences occurred in the past. During the seismic sequence, major west-dipping and minor conjugate east-dipping crustal faults activated accommodating an extension oriented ~EW, consistent with a tectonic regime of the area inferred from other seismic and structural observation in previous studies (Illsley-Kemp et al., 2018; Zwaan et al., 2020a). Deep seismicity focuses in a crust characterized by high Vp/Vs ratios and slow seismic velocities which could indicate the presence of partial melt or other fluids (Chambers et al., 2019; Hammond et al., 2011; Korostelev et al., 2015).

Our results support the hypothesis that extension is still ongoing in the NWAM and provide new constrains on the kinematics of previously poorly investigated areas of the margin, especially the marginal grabens. However, we also suggest that extension in the region near the Dergaha graben is accompanied by fluid induced faulting in the lower crust as indicated by the deep seismicity, the presence of hot springs, and by independent geophysical and geological evidences of partial melt beneath Dergaha (Figure 6) (Barberi, Borsi, et al., 1972; Chambers et al., 2019; Hammond et al., 2011; Korostelev et al., 2015; Tortelli et al., 2020). Such evidences could thus suggest that partial melt may play an important role in influencing the fault activity at the rift margins during incipient breakup in Northern Afar.

Data Availability Statement

The continuous seismic data used in this study are archived on the IRIS-DMC (http://www.fdsn.org/networks/detail/YQ_2017/; http://www.fdsn.org/networks/detail/YP_2017/). The data will become fully open access with the publication of this manuscript, or once the 3-years embargo period finishes at the end of 2021, whichever is sooner.

Acknowledgments
This study was developed in the framework of the PhD project of A. La Rosa (XXXIII cycle of the Dottorato Regionale Pegaso in Earth Sciences) and is supported by the Ministero Università e Ricerca (MiUR) through PRIN Grant 2017P9AT72. A. La Rosa and C. Pagli acknowledge partial support by the University of Pisa Grant PRA_2018_19. Sentinel-1 IW SLCs are provided by the Copernicus Open Access Hub (Sentinel-1) (https://scihub.copernicus.eu/). Shuttle Radar Topography Mission Digital Elevation Models (SRTM-DEM) can be downloaded from the U.S. Geological Survey Earth Explorer web service (https://earthexplorer.usgs.gov). Seismic instruments (USGS NEIC) were loaned by SEIS-UK. The facilities of SEIS-UK are supported by the Natural Environment Research Council (NERC) under agreement R8/H10/64. Instruments for the Southern profile belong to the French national pool of portable seismic instruments SISMOB-RESIF (INSU-CNRS). The temporary network deployments were part of an Actions-Marges and ISTeP project (#2016-82). We thank the regional authorities of the Afar, Tigray and Amhara for their administrative support. We also thank the wider staff body at the IGSSA of Addis Ababa University and the Centre Français d'Etudes Ethiopiennes (CFEE, IFRE23, USR3117) for the support in Ethiopia.

References

Albaric, J., Déverchère, J., Perrot, J., Jakovlev, A., & Deschamps, A. (2014). Deep crustal earthquakes in North Tanzania, East Africa: Interplay between tectonic and magmatic processes in an incipient rift. *Geochemistry, Geophysics, Geosystems*, *15*, 374–394. https://doi.org/10.1002/2013GC005027

Albaric, J., Déverchère, J., Petit, C., Perrot, J., & Le Gall, B. (2009). Crustal rheology and depth distribution of earthquakes: Insights from the central and southern East African Rift System. *Tectonophysics*, *468*(1–4), 28–41. https://doi.org/10.1016/j.tecto.2008.05.021

Antonioli, A., Piccinini, D., Chiaraluce, L., & Cocco, M. (2005). Fluid flow and seismicity pattern: Evidence from the 1997 Umbria-Marche (central Italy) seismic sequence. *Geophysical Research Letters*, *32*, L10311. https://doi.org/10.1029/2004GL022256

Ayalew, D., Ebinger, C., Bourdon, E., Wolfenden, E., Yirgu, G., & Grassineau, N. (2006). Temporal compositional variation of syn-rift rhyolites along the western margin of the southern Red Sea and northern Main Ethiopian Rift (Vol. 259, pp. 121–130). Geological Society Special Publication. https://doi.org/10.1144/gsl.sp.2006.259.01.10

Ayele, A., Stuart, G., Bastow, I., & Keir, D. (2007). The August 2002 earthquake sequence in north Afar: Insights into the neotectonics of the Danakil microplate. *Journal of African Earth Sciences*, *48*(2–3), 70–79. https://doi.org/10.1016/j.jafrearsci.2006.06.011

Baker, B. H., Mohr, P. A., & Williams, L. A. J. (1972). Geology of the Eastern Rift System of Africa (Vol. 136). Geological Society of America. https://doi.org/10.1130/SPE136-p1

Barberi, F., Borsi, S., Ferrara, G., Marinelli, G., Santacroce, R., Tazieff, H., & Varet, J. (1972). Evolution of the Danakil Depression (Afar, Ethiopia) in Light of Radiometric Age Determinations. *The Journal of Geology*, *80*, 720–729. https://doi.org/10.1086/627797

Barberi, F., Tazieff, H., & Varet, J. (1972). Volcanism in the Afar Depression: Its tectonic and magmatic significance. *Tectonophysics*, *15*(C), 19–29. https://doi.org/10.1016/0040-1951(72)90046-7

Belachew, M., Ebinger, C., Coté, D., Keir, D., Rowland, J. V., Hammond, J. O. S., & Ayele, A. (2011). Comparison of dike intrusions in an incipient seafloor-spreading segment in Afar, Ethiopia: Seismicity perspectives. *Journal of Geophysical Research*, *116*, B06405. https://doi.org/10.1029/2010JB007908

Beyene, A., & Abdelsalam, M. G. (2005). Tectonics of the Afar Depression: A review and synthesis. *Journal of African Earth Sciences*, *41*(1–2), 41–59. https://doi.org/10.1016/j.jafrearsci.2005.03.003

Blanchette, A. R., Klemperer, S. L., Mooney, W. D., & Zahran, H. M. (2018). Two-stage Red Sea rifting inferred from mantle earthquakes in Neoproterozoic lithosphere. *Earth and Planetary Science Letters*, *497*, 92–101. https://doi.org/10.1016/j.epsl.2018.05.048

Buck, W. R. (2006). The role of magma in the development of the Afro-Arabian Rift Systems. In G. Yirgu, C. J. Ebinger, & P. K. H. Maguire (Eds.), *The Afar Volcanic Province within the East African Rift System*, 259 (pp. 43–54). Geological Society, London, Special Publications. https://doi.org/10.1144/GSL.SP.2006.259.01.05

Chambers, E. L., Harmon, N., Keir, D., & Rychert, C. A. (2019). Using ambient noise to image the Northern East African rift. *Geochemistry, Geophysics, Geosystems*, *20*, 2091–2109. https://doi.org/10.1029/2018GC008129

Chorowicz, J., Collet, B., Bonavia, F., & Korme, T. (1999). Left-lateral strike-slip tectonics and gravity induced individualisation of wide continental blocks in the western Afar margin. *Eclogae Geologicae Helvetiae*, *92*(1), 149–158. https://doi.org/10.5169/seals-168656

Corti, G. (2009). Continental rift evolution: From rift initiation to incipient break-up in the Main Ethiopian Rift, East Africa. *Earth-Science Reviews*, *96*(1–2), 1–53. https://doi.org/10.1016/j.earscirev.2009.06.005

Craig, T. J., Jackson, J. A., Priestley, K., & Mckenzie, D. (2011). Earthquake distribution patterns in Africa: Their relationship to variations in lithospheric and geological structure, and their rheological implications. *Geophysical Journal International*, *185*(1), 403–434. https://doi.org/10.1111/j.1365-246x.2011.04950.x

Dawson, J., & Tregoning, P. (2007). Uncertainty analysis of earthquake source parameters determined from InSAR: A simulation study. *Journal of Geophysical Research*, *112*, B09406. https://doi.org/10.1029/2007JB005209

Déverchère, J., Petit, C., Gileva, N., Radziminovitch, N., Melnikova, V., & San'Kov, V. (2001). Depth distribution of earthquakes in the Baikal Rift System and its implications for the rheology of the lithosphere. *Geophysical Journal International*, *146*(3), 714–730. https://doi.org/10.1046/j.0956-540x.2001.1484.484.x

Doser, D. I., & Yarwood, D. R. (1994). Deep crustal earthquakes associated with continental rifts. *Tectonophysics*, *229*(1–2), 123–131. https://doi.org/10.1016/0040-1951(94)90008-6

Doubre, C., Leroy, S., Keir, D., Pagli, C., & RESIF. (2017). *Study of the structure of the lithosphere from the continental plateau of western Ethiopia to the active Afar rift (RESIF-SISMOB) [Data set]*. RESIF - Réseau Sismologique et géodésique Français. https://doi.org/10.15778/RESIF.YP2017

Doubre, C., & Peltzer, G. (2007). Fluid-controlled faulting process in the Asal Rift, Djibouti, from 8 yr of radar interferometry observations. *Geology*, *35*(1), 69–72. https://doi.org/10.1130/g23022a.1

Ebinger, C., & Belachew, M. (2010). Active passive margins. *Nature Geoscience*, *3*(10), 670–671. https://doi.org/10.1038/ngeo972

Ebinger, C. J., Keir, D., Ayele, A., Calais, E., Wright, T. J., Belachew, M., et al. (2008). Capturing magma intrusion and faulting processes during continental rupture: Seismicity of the Dabbahu (Afar) rift. *Geophysical Journal International*, *174*(3), 1138–1152. https://doi.org/10.1111/j.1365-246x.2008.03877.x

Farr, T. G., Rosen, P., Caro, E., Crippen, R., Duren, R., Hensley, S., et al. (2007). The Shuttle Radar Topography Mission. *Reviews of Geophysics*, *45*, RG2004. https://doi.org/10.1029/2005RG000183

Funning, G. J., & Garcia, A. (2019). A systematic study of earthquake detectability using Sentinel-1 Interferometric Wide-Swath data. *Geophysical Journal International*, *216*(1), 332–349. https://doi.org/10.1093/gji/ggy426

Goldstein, R. M., & Werner, C. L. (1998). Radar interferogram filtering for geophysical applications. *Geophysical Research Letters*, *25*(21), 4035–4038. https://doi.org/10.1029/1998GL900033

Goldstein, R. M., Zebker, H. A., & Werner, C. L. (1988). Satellite radar interferometry: Two-dimensional phase unwrapping. *Radio Science*, *23*(4), 713–720. https://doi.org/10.1029/RS023i004p00713

Gouin, P. (1979). *Earthquake history of Ethiopia and the Horn of Africa* (p. 259).Ottawa: International Development Research Centre.

Hammond, J. O. S., Kendall, J. M., Stuart, G. W., Keir, D., Ebinger, C., Ayele, A., & Belachew, M. (2011). The nature of the crust beneath the Afar triple junction: Evidence from receiver functions. *Geochemistry, Geophysics, Geosystems*, *12*, Q12004. https://doi.org/10.1029/2011GC003738

Hayward, N. J., & Ebinger, C. J. (1996). Variations in the along-axis segmentation of the Afar. *Tectonics*, *15*(2), 244–257. https://doi.org/10.1029/95TC02292

Illsley-Kemp, F., Keir, D., Bull, J. M., Gernon, T. M., Ebinger, C., Ayele, A., et al. (2018). Seismicity during continental breakup in the red sea rift of Northern Afar. *Journal of Geophysical Research: Solid Earth*, *123*, 2345–2362. https://doi.org/10.1002/2017JB014902

Illsley-Kemp, F., Savage, M. K., Keir, D., Hirschberg, H. P., Bull, J. M., Gernon, T. M., et al. (2017). Extension and stress during continental breakup: Seismic anisotropy of the crust in Northern Afar. *Earth and Planetary Science Letters*, *477*, 41–51. https://doi.org/10.1016/j.epsl.2017.08.014

Keir, D., Bastow, I. D., Pagli, C., & Chambers, E. L. (2013). The development of extension and magmatism in the Red Sea rift of Afar. *Tectonophysics*, *607*, 98–114. https://doi.org/10.1016/j.tecto.2012.10.015

Keir, D., Bastow, I. D., Whaler, K. A., Daly, E., Cornwell, D. G., & Hautot, S. (2009). Lower crustal earthquakes near the Ethiopian rift induced by magmatic processes. *Geochemistry, Geophysics, Geosystems*, *10*, Q0AB02. https://doi.org/10.1029/2009GC002382

Keir, D., Doubre, C., & Leroy, S. (2017). *Afar margin northern profile*. International Federation of Digital Seismograph Networks. https://doi.org/10.7914/SN/YQ_2017

Keranen, K., Klemperer, S. L., Gloaguen, R., Asfaw, L., Ayele, A., Ebinger, C., et al. (2004). Three-dimensional seismic imaging of a protoridge axis in the Main Ethiopian rift. *Geology*, *32*(11), 949–952. https://doi.org/10.1130/g20737.1

Korostelev, F., Weemstra, C., Leroy, S., Boschi, L., Keir, D., Ren, Y., et al. (2015). Magmatism on rift flanks: Insights from ambient noise phase velocity in Afar region. *Geophysical Research Letters*, *42*, 2179–2188. https://doi.org/10.1002/2015GL063259

Lapins, S., Kendall, J. M., Ayele, A., Wilks, M., Nowacki, A., & Cashman, K.V. (2020). Lower-crustal seismicity on the eastern border faults of the Main Ethiopian Rift. *Journal of Geophysical Research: Solid Earth*, *125*, e2020JB020030.

Lavayssière, A., Drooff, C., Ebinger, C., Gallacher, R., Illsley-Kemp, F., Oliva, S. J., & Keir, D. (2019). Depth extent and kinematics of faulting in the Southern Tanganyika Rift, Africa. *Tectonics*, *38*, 842–862. https://doi.org/10.1029/2018TC005379

Lee, H., Muirhead, J. D., Fischer, T. P., Ebinger, C. J., Kattenhorn, S. A., Sharp, Z. D., & Kianji, G. (2016). Massive and prolonged deep carbon emissions associated with continental rifting. *Nature Geoscience*, *9*(2), 145–149. https://doi.org/10.1038/ngeo2622

Lomax, A., Virieux, J., Volant, P., & Berge-Thierry, C. (2000). Probabilistic earthquake location in 3D and layered models. In C. H. Thurber, & N. Rabinowitz (Eds.), *Advances in seismic event location* (pp. 101–134). Berlin: Springer. https://doi.org/10.1007/978-94-015-9536-0_5

Maguire, P. K. H., Keller, G. R., Klemperer, S. L., Mackenzie, G. D., Keranen, K., Harder, S., et al. (2006). Crustal structure of the Northern Main Ethiopian Rift from the EAGLE controlled-source survey: A snapshot of incipient lithospheric break-up (Vol. 259, pp. 269–292). London: Geological Society, Special Publication. https://doi.org/10.1144/GSL.SP.2006.259.01.21

Makris, J., & Ginzburg, A. (1987). The Afar Depression: transition between continental rifting and sea-floor spreading. *Tectonophysics*, *141*(1–3), 199–214. https://doi.org/10.1016/0040-1951(87)90186-7

Manighetti, I., Tapponnier, P., Courtillot, V., Gallet, Y., Jacques, E., & Gillot, P.-Y. (2001). Strain transfer between disconnected, propagating rifts in Afar. *Journal of Geophysical Research*, *106*(B7), 13613–13665. https://doi.org/10.1029/2000JB900454

Mohr, P., & Gouin, P. (1976). Ethiopian Rift System. In C. L. Drake (Ed.), Geodynamics: Progress and prospects (Vol. 5, 81–87). Washington, DC: American Geophysical Union. https://doi.org/10.1029/SP005p0081

Muluneh, A. A., Brune, S., Illsley-Kemp, F., Corti, G., Keir, D., Glerum, A., et al. (2020). Mechanism for deep crustal seismicity: Insight from modeling of deformation processes at the Main Ethiopian Rift. *Geochemistry, Geophysics, Geosystems*, *21*, e2020GC008935. https://doi.org/10.1029/2020GC008935

Okada, Y. (1985). Surface deformation due to shear and tensile faults in a half-space. *Bulletin of the Seismological Society of America*, *75*(4), 1135–1153.

Pagli, C., Wang, H., Wright, T. J., Calais, E., & Lewi, E. (2014). Current plate boundary deformation of the Afar rift from a 3-D velocity field inversion of InSAR and GPS. *Journal of Geophysical Research: Solid Earth*, *119*, 8562–8575. https://doi.org/10.1002/2014JB011391

Pallister, J. S., McCausland, W. A., Jónsson, S., Lu, Z., Zahran, H. M., Hadidy, S. E., et al. (2010). Broad accommodation of rift-related extension recorded by dyke intrusion in Saudi Arabia. *Nature Geoscience*, *3*(10), 705–712. https://doi.org/10.1038/ngeo966

Rosen, P. A., Gurrola, E. M., Sacco, G. F., & Zebker, H. (2012). The InSAR scientific computing environment. In *EUSAR*; 9th European Conference on Synthetic Aperture Radar (pp. 730–733).

Sembroni, A., Molin, P., Dramis, F., Faccenna, C., & Abebe, B. (2017). Erosion-tectonics feedbacks in shaping the landscape: An example from the Mekele Outlier (Tigray, Ethiopia). *Journal of African Earth Sciences*, *129*, 870–886. https://doi.org/10.1016/j.jafrearsci.2017.02.028

Seno, T., & Saito, A. (1994). Recent East African earthquakes in the lower crust. *Earth and Planetary Science Letters*, *121*, 125–136. https://doi.org/10.1016/0012-821X(94)90036-1

Shudofsky, G. N. (1985). Source mechanisms and focal depths of East African earthquakes using Rayleigh-wave inversion and body-wave modelling. *Geophysical Journal International*, *83*(3), 563–614. https://doi.org/10.1111/j.1365-246x.1985.tb04328.x

Snoke, J. A. (2003). 85.12 FOCMEC: FOCal MEChanism determinations. *International Geophysics*, *81*(Part B), 1629–1630. https://doi.org/10.1016/s0074-6142(03)80291-7

Stab, M., Bellahsen, N., Pik, R., Quidelleur, X., Ayalew, D., & Leroy, S. (2016). Modes of rifting in magma-rich settings: Tectono-magmatic evolution of Central Afar. *Tectonics*, *35*, 2–38. https://doi.org/10.1002/2015TC003893

Tesfaye, S., & Ghebreab, W. (2013). Simple shear detachment fault system and marginal grabens in the southernmost Red Sea rift. *Tectonophysics*, *608*, 1268–1279. https://doi.org/10.1016/j.tecto.2013.06.014

Tortelli, G., Gioncada, A., Pagli, C., Rosi, M., Keir, D., & De Dosso, L. (2020). Evidence of active magmatic rifting in Ma'alalta marginal volcano (Afar, Ethiopia). *EGU General Assembly*. Online, 4–8 May 2020, EGU2020-6976 https://doi.org/10.5194/egusphere-egu2020-6976

Waldhauser, F. (2001). hypoDD: A computer program to compute double-difference hypocenter locations. *U.S. Geological Survey Open-File Report, 01–113*, 25

Waldhauser, F., & Ellsworth, W. L. (2000). A double-difference earthquake location algorithm: Method and application to the Northern Hayward Fault, California. *Bulletin of the Seismological Society of America*, *90*(6), 1353–1368. https://doi.org/10.1785/0120000006

Wolfenden, E., Ebinger, C., Yirgu, G., Renne, P. R., & Kelley, S. P. (2005). Evolution of a volcanic rifted margin: Southern Red Sea, Ethiopia. *Geological Society of America Bulletin*, *117*(7–8), 846–864. https://doi.org/10.1130/b25516.1

Wright, T. J., Ebinger, C., Biggs, J., Ayele, A., Yirgu, G., Keir, D., & Stork, A. (2006). Magma-maintained rift segmentation at continental rupture in the 2005 Afar dyking episode. *Nature*, *442*(7100), 291–294. https://doi.org/10.1038/nature04978

Wright, T. J., Sigmundsson, F., Pagli, C., Belachew, M., Hamling, I. J., Brandsdóttir, B., et al. (2012). Geophysical constraints on the dynamics of spreading centres from rifting episodes on land. *Nature Geoscience*, *5*(4), 242–250. https://doi.org/10.1038/ngeo1428

Yamada, T., Yukutake, Y., Terakawa, T., & Arai, R. (2015). Migration of earthquakes with a small stress drop in the Tanzawa Mountains, Japan. *Earth, Planets and Space*, *67*, 175. https://doi.org/10.1186/s40623-015-0344-6

Yoshida, K., & Hasegawa, A. (2018). Hypocenter migration and seismicity pattern change in the Yamagata-Fukushima Border, NE Japan, caused by fluid movement and pore pressure variation. *Journal of Geophysical Research: Solid Earth*, *123*, 5000–5017. https://doi.org/10.1029/2018JB015468

Zwaan, F., Corti, G., Keir, D., & Sani, F. (2020). A review of tectonic models for the rifted margin of Afar: Implications for continental break-up and passive margin formation. *Journal of African Earth Sciences*. *164*, 103649. https://doi.org/10.1016/j.jafrearsci.2019.103649

Zwaan, F., Corti, G., Sani, F., Keir, D., Muluneh, A., Illsley-Kemp, F., & Papini, M. (2020a). Structural analysis of the Western Afar Margin, East Africa: Evidence for multiphase rotational rifting. *Tectonics*, *39*, e2019TC006043. https://doi.org/10.1029/2019tc006043

Zwaan, F., Corti, G., Sani, F., Keir, D., Muluneh, A., Illsley-Kemp, F., & Papini, M. (2020b). *Geological data from the western Afar margin, East Africa*. GFZ Data Services. http://doi.org/10.5880/fidgeo.2020.017